Electromagnetic Modeling of Plasma Etch Chamber for Semiconductor Microchip Fabrication

Zhigang Chen, **Shahid Rauf**, **Kartik Ramaswamy**, **and Ken Collins**
Applied Materials, Inc., Sunnyvale, California 94085, USA

Abstract— In the plasma etch chamber used to fabricate semiconductor microchips, maintaining the symmetry and uniformity of the electric field in the plasma discharge region is critical. Very-high-frequency (VHF) RF sources are attractive for such applications as they improve the efficiency of plasma generation. Electromagnetic effects become important at these frequencies, and etch chamber design requires careful investigation of the electromagnetic field spatial structure in the chamber. In this paper, we apply the finite-difference time-domain (FDTD) method to examine various electromagnetic effects in the plasma etch chamber and investigate strategies for improved chamber design. These effects include the standing wave effects and asymmetric field distributions that can be caused by asymmetric RF power feed configurations. The FDTD method is formulated in both cylindrical and Cartesian coordinate systems to facilitate modeling of rotationally symmetric chamber and asymmetric RF feed structures. The electric field distribution generated by various RF feed configurations is studied at different VHF frequencies. Based on the FDTD simulations, we have been able to identify a variety of design approaches for ensuring electric field symmetry and uniformity.

1. INTRODUCTION

Radio frequency (RF) capacitively coupled plasma discharges are widely used in semiconductor microchip fabrication for plasma etching [1]. In such plasma etching reactors, the plasma is generated by applying a sinusoidal RF signal to two parallel circular electrodes spaced by a few centimeters. The RF power is guided to the electrodes via a coaxial line, and the whole system is enclosed by a cylindrical metal chamber. Initially, discrete frequencies between 2–30 MHz were used for plasma processing. To increase the power coupling efficiency to the plasma, VHF sources ranging from 30–162 MHz have since become popular. However, the excitation frequency cannot be increased indefinitely since major processing uniformity issues arise when electromagnetic effects are significant. That is, when the RF wavelength becomes comparable to the chamber dimension, which is ~ 500 mm for a semiconductor wafer size of 300 mm, and the plasma skin depth becomes comparable to the electrode size and spacing.

When the electromagnetic effects become significant, it is indispensable to fully understand the electrodynamic behavior of the RF fields in the etch chambers because any nonuniformity of the electric fields in the plasma region would directly have an impact on the etch uniformity and quality. In this paper, we apply the FDTD technique [2] to model the RF wave behavior in the chamber. We particularly pay attention to the electric field distribution at the wafer level and the corresponding electromagnetic effects at very high frequency. The FDTD method is formulated in both cylindrical and Cartesian coordinate systems to facilitate modeling of rotationally symmetric chamber and asymmetric RF feed structures. We couple the FDTD formulation with the CPML [2] absorbing boundary conditions to accurately simulate the RF power delivery via a coaxial line.

2. COMPUTATIONAL METHOD DESCRIPTION

To make the computational model conformal to the geometrical features in the cylindrical etching chamber, we formulate the FDTD method in the cylindrical coordinate system. In the cylindrical coordinate system, the Maxwell's curl equations for linear, isotropic, nondispersive materials can

be written as:

$$\frac{\partial E_r}{\partial t} = \frac{1}{\varepsilon}\left(\frac{1}{r}\frac{\partial H_z}{\partial \phi} - \frac{\partial H_\phi}{\partial z}\right) - \frac{\sigma}{\varepsilon}E_r \tag{1}$$

$$\frac{\partial E_\phi}{\partial t} = \frac{1}{\varepsilon}\left(\frac{\partial H_r}{\partial z} - \frac{\partial H_z}{\partial r}\right) - \frac{\sigma}{\varepsilon}E_\phi \tag{2}$$

$$\frac{\partial E_z}{\partial t} = \frac{1}{\varepsilon}\left[\frac{1}{r}\frac{\partial (rH_\phi)}{\partial r} - \frac{1}{r}\frac{\partial H_r}{\partial \phi}\right] - \frac{\sigma}{\varepsilon}E_z \tag{3}$$

$$\frac{\partial H_r}{\partial t} = \frac{1}{\mu}\left(\frac{\partial E_\phi}{\partial z} - \frac{1}{r}\frac{\partial E_z}{\partial \phi}\right) \tag{4}$$

$$\frac{\partial H_\phi}{\partial t} = \frac{1}{\mu}\left(\frac{\partial E_z}{\partial r} - \frac{\partial E_r}{\partial z}\right) \tag{5}$$

$$\frac{\partial H_z}{\partial t} = \frac{1}{\mu}\left[\frac{1}{r}\frac{\partial E_r}{\partial \phi} - \frac{1}{r}\frac{\partial (rE_\phi)}{\partial r}\right] \tag{6}$$

Discretizing Eqs. (1)–(6) using the conventional Yee lattice, we can obtain the corresponding finite-difference equations. For example, the finite-difference equation for E_z is given by

$$E_z|_{i,j,k+1/2}^{n+1} = \left(\frac{1-\frac{\sigma_{i,j,k+1/2}\Delta t}{2\varepsilon_{i,j,k+1/2}}}{1+\frac{\sigma_{i,j,k+1/2}\Delta t}{2\varepsilon_{i,j,k+1/2}}}\right)E_z|_{i,j,k+1/2}^{n} + \left(\frac{\frac{\Delta t}{\varepsilon_{i,j,k+1/2}}}{1+\frac{\sigma_{i,j,k+1/2}\Delta t}{2\varepsilon_{i,j,k+1/2}}}\right)\left[\begin{array}{l}\left(\frac{1}{2r_i}+\frac{1}{\Delta r}\right)H_\phi\Big|_{i+1/2,j,k+1/2}^{n+1/2} \\ +\left(\frac{1}{2r_i}-\frac{1}{\Delta r}\right)H_\phi\Big|_{i-1/2,j,k+1/2}^{n+1/2} \\ +\frac{H_r|_{i,j-1/2,k+1/2}^{n+1/2} - H_r|_{i,j+1/2,k+1/2}^{n+1/2}}{r_i\Delta\phi}\end{array}\right] \tag{7}$$

In cylindrical coordinate system, the time step required to ensure numerical stability is given by

$$\Delta t \le \frac{1}{c\sqrt{(1/\Delta r)^2 + \left[1/(r_{\min}\Delta\phi)\right]^2 + (1/\Delta z)^2}}, \tag{8}$$

where $r_{\min} = 0.5\Delta r$.

E_z is required to be evaluated along the z-axis where $r = 0$ and direct use of Eq. (7) would encounter singularities. To determine E_z along the z-axis, we start with the integral form of Ampere's law of Maxwell's equations:

$$\oint_C \mathbf{H}\cdot d\mathbf{l} = \int_S \left(\varepsilon\frac{\partial \mathbf{E}}{\partial t} + \sigma\mathbf{E}\right)\cdot d\mathbf{s}, \tag{9}$$

where C is a closed contour around the z-axis and S is the surface bounded by the contour C. Choosing the smallest contour around the z-axis that has a radius of $0.5\Delta r$, we obtain

$$E_z|_{0,j,k+1/2}^{n+1} = \left(\frac{1-\frac{\sigma_{0,j,k+1/2}\Delta t}{2\varepsilon_{0,j,k+1/2}}}{1+\frac{\sigma_{0,j,k+1/2}\Delta t}{2\varepsilon_{0,j,k+1/2}}}\right)E_z|_{0,j,k+1/2}^{n} + \left(\frac{\frac{2\Delta t\Delta\phi}{\varepsilon_{i,j,k+1/2}\pi\Delta r}}{1+\frac{\sigma_{i,j,k+1/2}\Delta t}{2\varepsilon_{i,j,k+1/2}}}\right)\sum_{j=0}^{N_\phi-1} H_\phi|_{1/2,j,k+1/2}^{n+1/2}, \tag{10}$$

where N_ϕ is the number of grid points along the azimuthal direction.

To accurately model the propagating TEM wave behavior in a coaxial line, we apply the CPML to truncate the coaxial line in the z-direction. The details of the CPML implementation can be found in [2].

The plasma etching chamber usually operates at discrete frequencies. Therefore, we excite the system using a monochromatic sinusoidal current source. The current source is designed to excite the TEM mode in the coaxial line. In a coaxial line, the TEM mode is defined by [3]

$$E_r = \frac{V(t)}{\ln(b/a)}\frac{1}{r}, \quad H_\phi = \frac{V(t)}{\eta\ln(b/a)}\frac{1}{r} \tag{11}$$

where $V(t)$ is the applied voltage, a and b are the radii of the inner and outer conductors, respectively, and η is the intrinsic impedance of the insulating material in the coaxial line. The

corresponding current sheet density on a $z = z_0$ plane based on the surface equivalence theorem is given by

$$J_r = -H_\phi = -\frac{V(t)}{\eta \ln(b/a)} \frac{1}{r} \tag{12}$$

This current sheet source is applied to a cross section of the coaxial line about 5 cells away from the PML.

To decrease the transient time in a single frequency simulation, we choose a new time function based on the Hanning window function to replace the stepped monochromatic excitation [4]:

$$V(t) = \begin{cases} 0.5 \sin(2\pi f t)[1 - \cos(\frac{\pi t}{T})], & 0 \le t \le T \\ \sin(2\pi f t), & t > T \end{cases} \tag{13}$$

where T is the rising time that can be taken to be several cycles of the excitation frequency.

3. RESULTS AND DISCUSSIONS

A simplified model for a plasma etch chamber is shown in Fig. 1. Fig. 1(a) shows the internal structures of the chamber whereas Fig. 1(b) presents a cross-sectional view. The RF power is delivered into the chamber via a coaxial line. The inner conductor of the coaxial line to which the RF voltage is applied is connected to the bottom electrode. Above the bottom electrode is the electrostatic "chuck" which makes use of the electrostatic force to hold a semiconductor wafer on it. The outer conductor of the coaxial line is connected to a grounded metal plate and chamber wall. The grounded metal plate and the RF "hot" electrode are separated by quartz. Between the electrostatic chuck and the top grounded electrode is the plasma region. A thin plasma sheath between 1 mm–1 cm is usually formed between plasma and wafer. The ions are accelerated by the electric field in the plasma sheath and will bombard the wafer with a significant energy to facilitate the etching process. The uniformity of the electric field distribution within the plasma sheath therefore would directly impact the etch rate uniformity. We investigate how the electric field distribution in the plasma sheath changes as we increase the RF frequency and as the plasma conductivity changes.

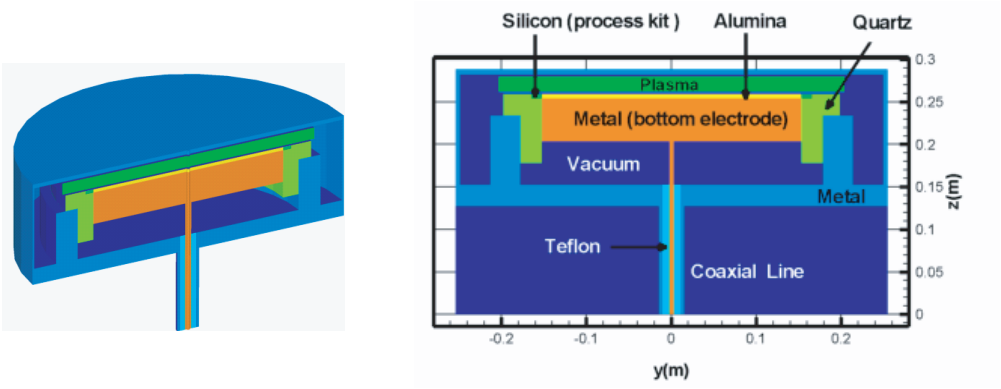

Figure 1: A simplified model for a plasma etching chamber. (a) The internal view of the chamber. (b) The cross-sectional view of the chamber.

We run the FDTD simulations for a mesh of $102 \times 36 \times 230$ cells for a number of periods until they reach steady state. Then we take discrete Fourier transform of the time-domain data to obtain the electric field at a given frequency. To facilitate the studies of the electromagnetic effects, we first treat plasma as a linear lossy medium with constant conductivity of 1 S/m and the plasma sheath as a vacuum gap of 2.5 mm. The chosen conductivity corresponds to a plasma density of about 1×10^{16} m^{-3}and collision frequency of about 3×10^8 s^{-1}. The discrete frequencies we have investigated are 13.56 MHz and 60 MHz. The electric field distributions at the wafer level (i.e., the electric field between plasma and electrostatic chuck) are shown on Fig. 2 where we have normalized the electric field by its maximum. Note that we have used different color scales for each frequency in order to amplify the nonuniformity within the boundary of a wafer (the black circle in the figure). Fig. 2(a) shows the electric field at 13.56 MHz. We see that the electric

field distribution at this frequency is uniform within the boundary of a wafer because the effective wavelength is large compared to the chamber dimensions. However, the electric field decays rapidly after passing the edge of the bottom electrode. Fig. 2(b) shows the electric field at 60 MHz. At this frequency, the effective wavelength is still large compared to the chamber dimensions. However, the skin depth of the plasma with 1 S/m conductivity is 6.5 cm and is comparable to the wafer radius. This skin effects lead to an edge-high and center-low pattern as shown in Fig. 2(b). We note that the nonuniformity caused by the skin effects is small ($< 1\%$). Fig. 2(c) shows the electric field at 60 MHz, but for 10 S/m plasma conductivity and 1.3 mm plasma sheath thickness. At such a high conductivity, the standing wave effects come into play even at 60 MHz and are dominant, leading to a center-high and edge-low pattern as shown in Fig. 2(c). We note that the lossy nature of the plasma can reduce the effective wavelength [3] and therefore make the standing wave effects more pronounced for high conductivity even at lower frequencies.

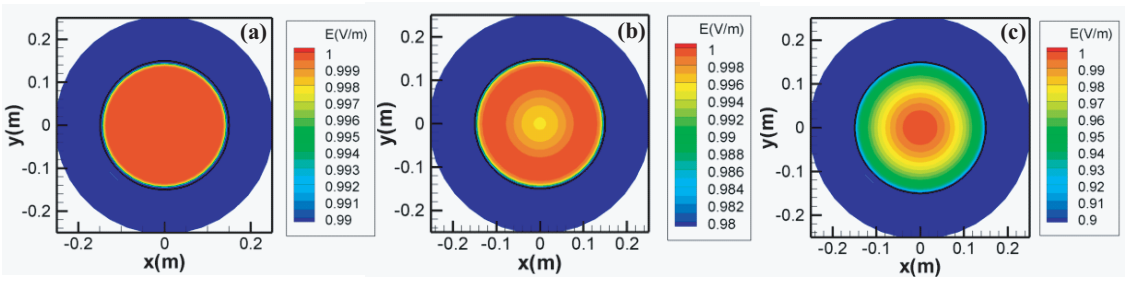

Figure 2: Electric field distribution 1 mm above the wafer level. The black circle denotes the boundary of a wafer. (a) 13.56 MHz (plasma conductivity = 1 S/m, plasma sheath thickness = 2.5 mm); (b) 60 MHz (plasma conductivity = 1 S/m, plasma sheath thickness = 2.5 mm); (c) 60 MHz (plasma conductivity = 10 S/m, plasma sheath thickness = 1.3 mm).

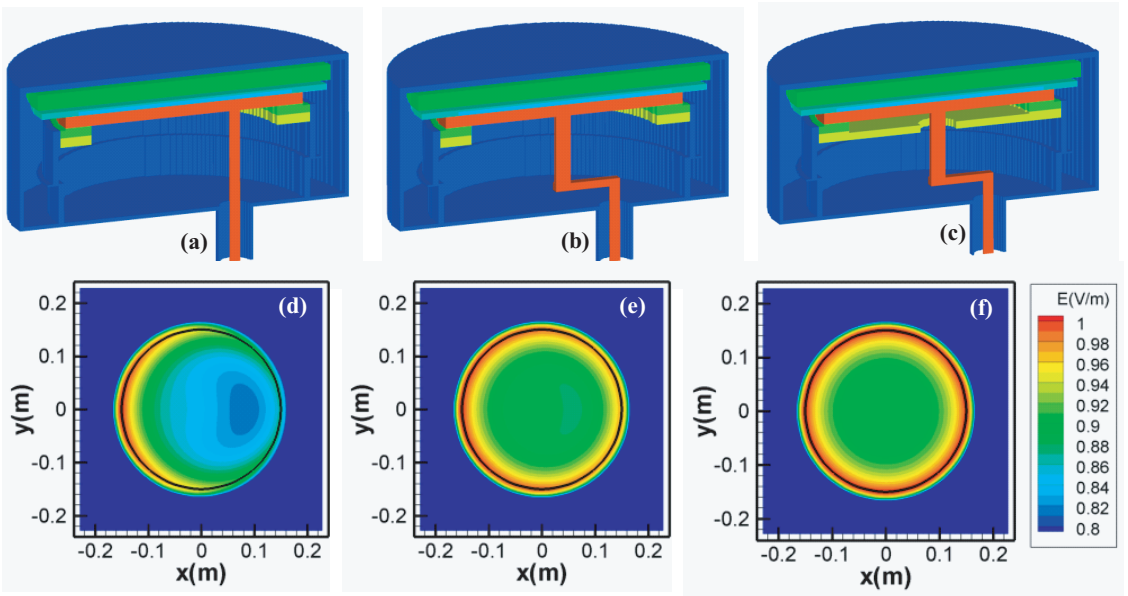

Figure 3: Three different RF feed configurations and the corresponding electric field distribution 1 mm above the wafer level at 60 MHz. Left: RF feed is about 7 cm off center; Middle: Center RF feed with off-center bend connected to power source; Right: Center RF feed with shielding grounded plate and off-center bend.

We also have studied the asymmetric field distributions that can be caused by asymmetric RF feed configurations in the chamber. Fig. 3 shows three different RF feed configurations and the corresponding electric field distribution 1 mm above the wafer level at 60 MHz. Here, we assume the plasma conductivity and sheath thickness are 0.1 S/m and 2.5 mm, respectively. These parameters correspond to a plasma density of about 1×10^{15} m^{-3}and collision frequency of about 3×10^{8} s^{-1}. The off-center RF feed in Fig. 3(a) causes significant asymmetric field distribution

shown in Fig. 3(d). Such asymmetric field distribution is not desired. One quick way to correct this problem is to use a bend structure to feed to the center of the bottom electrode, as shown in Fig. 3(b). Such a modification can significantly improve the field symmetry and uniformity as shown in Fig. 3(e). Further improvement can be achieved by adding a grounded metal plate (the yellow plate in Fig. 3(c)) above the RF bend. The grounded metal plate acts like a shield, and therefore minimizes the impact of the RF bend structure. The corresponding electric field distribution is quite uniform and symmetric, as shown in Fig. 3(f).

4. CONCLUSIONS

In summary, we have demonstrated electromagnetic modeling of plasma etching chamber based on FDTD method and evaluated the standing wave effects, the skin effects of the plasma and the asymmetric field distributions caused by asymmetric RF feed configurations in the chamber. Based on the FDTD simulations, we have been able to identify a variety of design approaches for ensuring electric field symmetry and uniformity. These design approaches are the foundation of new RF feed designs in our plasma etching chambers.

REFERENCES

1. Lieberman, M. A. and A. J. Lichtenberg, *Principles of Plasma Discharges and Materials Processing*, Wiley-Interscience, New Jersey, 2005.
2. Taflove, A. and S. C. Hagness, *Computational Electrodynamics: The Finite-Difference Time-Domain Method*, Artech House, Massachusetts, 2005.
3. Ramo, S., J. R. Whinnery, and T. V. Duzer, *Fields and Waves in Communication Electronics*, John Wiley & Sons, 1994.
4. Prescott, D. T. and N. V. Shuley, "Reducing solution time in monochromatic FDTD waveguide simulations," *IEEE Trans. Microw. Theory Tech.*, Vol. 42, No. 8, 1582–1584, 1994.